THE JOURNAL OF NAVIGATION (2019), **72**, 1633–1648. © The Royal Institute of Navigation 2019
doi:10.1017/S0373463319000274

Evaluation and Application of the GPS Code Observable in Precise Point Positioning

Haojun Li, Jingxin Xiao and Bofeng Li

(*College of Surveying and Geo-Informatics, Tongji University, Shanghai, 200092, P. R. China*)
(E-mail: bofeng_li@tongji.edu.cn)

The accuracy of the Global Positioning System (GPS) observable, especially for the code observable, has improved with the development of Global Navigation Satellite System (GNSS) receiver technology. An evaluation of the GPS code observable is presented in this paper, together with a stochastic model for the code and phase observables in Precise Point Positioning (PPP), established using the evaluated results. The results show that the code observables of Leica GNSS receivers are generally better than those of some other brand receivers and the Root Mean Square (RMS) for the code observables of the Leica GRX1200PRO, which includes the multipath effect, reaches 0·71 m, although Coarse/Acquisition (C/A) code observables are tracked. The static positioning of the code observable can reach centimetre level and the convergence time for the JPLM station is just 2·5 hours. The positioning results show that it is difficult to converge the Up direction to the centimetre level, compared with the North and East directions. The results show that static positioning can be correlated with the accumulation characteristic of the error for the code observable, while that that of the kinematic mode can be correlated to the error value. The shortened PPP convergence times verify that the presented stochastic models are effective.

KEYWORDS

1. Code observable. 2. Precise Point Positioning (PPP). 3. Stochastic model.

Submitted: 2 December 2018. Accepted: 29 March 2019. First published online: 2 May 2019.

1. INTRODUCTION. In Global Navigation Satellite System (GNSS) applications, for example, positioning and timing, two types of phase and code observables are used. The observables are deduced from measured time or phase differences based on a comparison between received signals and receiver-generated signals. The accuracies of these observables are dominated by the performance of the GNSS satellite and receiver. The impact of the code observable on positioning cannot be ignored (Banville et al., 2013; Li et al., 2016), although the accuracy of the phase observable is better than that of the code observable and the phase and code observables are generally used in high-precision and fast positioning. The original Global Positioning System (GPS) design contains two codes: the Coarse/Acquisition (C/A) code, which is freely available to the public, and the Precision

https://doi.org/10.1017/S0373463319000274 Published online by Cambridge University Press

(P) code, usually reserved for military applications. The major difference between the expressions of phase and code observables is the presence of the phase ambiguity in the code observable. Estimation of the phase ambiguity complicates the positioning processing when the phase observation is used.

It is considered that GNSS positioning has two positioning modes, which are the single-receiver observation-based point positioning and double-differenced-based relative positioning. Point positioning, the type of solution the GPS system was originally designed for, achieves a position accuracy of about 1 m (Leick et al., 2015). In the original point positioning processing systems, the receiver coordinates are estimated using the code observable and the satellite positions and satellite clock corrections from the broadcast ephemeris and navigation message. It is apparent that the accuracy of point positioning depends on the quality of the code observable and the serviced products of the satellite clock errors and orbits. The high-precision products of satellite clock errors and orbits are then estimated and provided by the International GNSS Service (IGS) (Dow et al., 2009) to meet the needs of high-precision point positioning. Based on the serviced precise products of satellite clock errors and orbits and the dual-frequency phase and code observations of a single receiver, Precise Point Positioning (PPP) (Zumberge et al., 1997) is realised. PPP has been demonstrated as a valuable technique for single-receiver positioning over a continental and even a global scale (Kouba, 2005; Leandro et al., 2011). It has been considered as an effective tool for many fields, for example the precise orbit determination of low Earth orbits (Bock et al., 2009), real-time water vapour estimation (Li et al., 2012) and determination of earthquake magnitude (Fang et al. 2014; Geng et al., 2016). In the past two decades, studies on PPP have covered accuracy analysis (Kouba and Héroux, 2001; Gao and Shen, 2002; Leandro et al., 2011), realisation of real-time PPP (Li et al., 2010a; 2010b; Shi et al., 2017) and PPP ambiguity (Laurichesse and Mercier, 2007; Collins, 2008; Ge et al., 2008; Geng et al., 2010; Teunissen et al., 2010; Loyer et al., 2012; Lannes and Prieur, 2013; Zhang et al., 2013; Teunissen and Khodabandeh, 2015). In current PPP processing schemes, the phase and code observables are used and different weights for the code and phase observables are set to prevent the code observable from affecting the estimated parameters.

With the development of GNSS satellite and receiver technology, the qualities of the observables have been improved significantly, especially the code observable. There are limited corresponding studies on accuracy analysis of the code observable and its performances in PPP, although the effect of the code observable on PPP has been analysed (Li et al., 2016). In addition, the studies by Wang et al. (1998), Li et al. (2008), Seepersad and Bisnath (2015) and Li et al. (2016) advise that weight setting is very important and that reasonable weights should be applied to obtain optimal solutions. The ratio of the standard deviations for the ionosphere-free carrier and code combinations, for example 1:100 (Hauschild and Montenbruck, 2009; Zhang et al., 2011), is generally determined according to previous experience. The same ratios of the standard deviations for all observation stations are used and this setting ignores the accuracy differences of the observables selected from different receivers in current GNSS processing. However, the accuracy of the observables is affected by the space environment and the accuracy of different stations varies, especially for the code observables. The accuracy of the observables depends to some extent on the technology of the GNSS receiver. Thus, the code observable should be reassessed and the ratio of the standard deviations for the ionosphere-free carrier and code combinations needs to be reset.

https://doi.org/10.1017/S0373463319000274 Published online by Cambridge University Press

Considering the above discussions, a method for evaluating the accuracy of the code observable is presented and the evaluated results are used to improve the random model of the code and phase observables-based conventional PPP. Meanwhile, the realisation of code observable-based PPP, in which only the code observable is used, is also discussed. The evaluation of the code observable is implemented, and the performance of the code observable-based PPP is then analysed using GPS dual-frequency data. Code and phase observables-based PPP is implemented based on a constructed stochastic model and its performance is validated using the collected data.

2. METHOD AND STRATEGY.

Generally, the quality of the code observable is evaluated using a multipath combination of the code and phase observables (Estey and Meertens, 1999; Hilla and Cline, 2004). In these studies, the phase observables are considered as the value which is not affected by noise. Considering application of the ionosphere-free combinations in PPP user and PPP service sides, the residual of the difference between the ionosphere-free carrier and code combinations is used to analyse the accuracy of the code observation. Then, the realisation of code observable-based PPP is discussed and a stochastic model for the phase and code observables based conventional PPP is developed.

2.1. *Evaluation of the GPS code observable.*

For a dual-frequency user, the ionosphere-free carrier (L1/L2) and code (P1/P2) combinations can be formed:

$$\begin{aligned} IF(L_1,L_2) &= \rho + \delta^r - \delta^s + \left(\frac{f_1^2}{f_1^2-f_2^2}N_1\lambda_1 - \frac{f_2^2}{f_1^2-f_2^2}N_2\lambda_1\right) \\ &\quad - \left(\frac{f_1^2}{f_1^2-f_2^2}FCB_1^r - \frac{f_2^2}{f_1^2-f_2^2}FCB_2^r\right) \\ &\quad + \left(\frac{f_1^2}{f_1^2-f_2^2}FCB_1^s - \frac{f_2^2}{f_1^2-f_2^2}FCB_2^s\right) - T + \varepsilon_{1,2} \\ IF(P_1,P_2) &= \rho + \delta^r - \delta^s - \left(\frac{f_1^2}{f_1^2-f_2^2}b_1^r - \frac{f_2^2}{f_1^2-f_2^2}b_2^r\right) \\ &\quad + \left(\frac{f_1^2}{f_1^2-f_2^2}b_1^s - \frac{f_2^2}{f_1^2-f_2^2}b_2^s\right) - T + \omega_{1,2} \end{aligned} \tag{1}$$

where ρ is the satellite-to-receiver range; T is tropospheric delay; f_i $(i = 1, 2)$ are the carrier frequencies of L1 and L2; N_i^s $(i = 1, 2)$ are the integral ambiguities of L1 and L2, and their wavelengths are λ_i $(i = 1, 2)$; FCB_i^s $(i = 1, 2)$ are the satellite Fractional Cycle Biases (FCBs) of L1 and L2 observations, FCB_i^r $(i = 1, 2)$ are the receiver FCBs; δ^r and δ^s are the receiver and satellite clock errors in metres, $b_i^s (i = 1, 2)$ are the satellite hardware delay biases of P1 and P2, $b_i^r (i = 1, 2)$ are the receiver hardware delay biases of P1 and P2 observations and $\varepsilon_{1,2}$ and $\omega_{1,2}$ are the signal noises of L1/L2 and P1/P2. The difference between L1/L2 and P1/P2 is written as:

$$\begin{aligned} &IF(L_1,L_2) - IF(P_1,P_2) \\ &= \left(\frac{f_1^2}{f_1^2-f_2^2}N_1\lambda_1 - \frac{f_2^2}{f_1^2-f_2^2}N_2\lambda_1\right) - \left(\frac{f_1^2}{f_1^2-f_2^2}FCB_1^r - \frac{f_2^2}{f_1^2-f_2^2}FCB_2^r\right) \end{aligned}$$

https://doi.org/10.1017/S0373463319000274 Published online by Cambridge University Press

$$+\left(\frac{{f_1}^2}{{f_1}^2-{f_2}^2}FCB_1^s-\frac{{f_2}^2}{{f_1}^2-{f_2}^2}FCB_2^s\right)-\left(\frac{{f_1}^2}{{f_1}^2-{f_2}^2}b_1^r-\frac{{f_2}^2}{{f_1}^2-{f_2}^2}b_2^r\right)$$
$$+\left(\frac{{f_1}^2}{{f_1}^2-{f_2}^2}b_1^s-\frac{{f_2}^2}{{f_1}^2-{f_2}^2}b_2^s\right)+\varepsilon_{1,2}-\omega_{1,2} \tag{2}$$

The standard deviation of the difference between the L1/L2 and P1/P2 is written as:

$$\sigma_{dif}=\sqrt{\sigma_{ifp}^2+\sigma_{ifc}^2} \tag{3}$$

where σ_{ifp}^2 and σ_{ifc}^2 are the variances for the L1/L2 and P1/P2, respectively. Equation (2) shows that the satellite and the receiver FCBs and the hardware delay are absorbed by the phase ambiguity, receiver clock and satellite clock, and the corresponding phase ambiguity values are constant. Assuming there is no cycle slip in m epochs, the residual of the differenced ionosphere-free carrier and code combinations is written as:

$$\Delta_j=((IF(L_1,L_2)-IF(P_1,P_2))_j-\left(\sum_{j=1}^{m}w_j\left((IF(L_1,L_2)-IF(P_1,P_2))_j\Big/\sum_{j=1}^{m}w_j\right)\right. \tag{4}$$

where w_j is the weight of the difference between L1/L2 and P1/P2. The elevation-dependent function is as follows:

$$w_j=\begin{Bmatrix}1 & 30^0\le\theta_j\le 90^0\\ 2\sin(\theta_j) & 10^0\le\theta_j<30^0\end{Bmatrix} \tag{5}$$

where θ_j is the satellite elevation at epoch j. Then, the RMS for the residuals of the differenced ionosphere-free carrier and code combinations is computed as:

$$\sigma_{dif}=\sqrt{\left(\sum_{j=1}^{m}\Delta_j^2\right)\Big/m} \tag{6}$$

The accuracy of the code observable is evaluated using the computed RMS of the residuals for the differenced ionosphere-free carrier and code combinations. For a GNSS receiver, n satellites are tracked, and the accuracy of the code observable is evaluated using the mean RMS:

$$\sigma_r=\sum_{i=1}^{n}\left(\sigma_{dif}\right)_i/n \tag{7}$$

The method for analysing the accuracy of the code observation, which uses the differenced ionosphere-free carrier and code combinations, considers that the same products of satellite orbits and clocks are used in the L1/L2 and P1/P2 at the PPP user side. This also ensures that the evaluated results are not affected by the serviced products of the precise satellite orbits and clocks.

2.2. *Code observable-based PPP.* Conventional PPP is realised based on dual-frequency ionosphere-free carrier and code combinations. The estimated parameters of the phase and code-based conventional PPP are receiver position, receiver clock error,

https://doi.org/10.1017/S0373463319000274 Published online by Cambridge University Press

Table 1. Settings for the code observable-based PPP processing.

Model		Settings
Measurements	Ionosphere-free code combination	
	Adjustment	Least square filter
	Weighting	Elevation-dependent function
Corrections	DCB(P1-C1)	Products provided by CODE
	Tides corrections	Solid tide and Ocean tide correction
	PCV	Absolute IGS 08 correction mode
	Relativity	Corrected
Parameters	Station coordinates	Estimated
	Troposphere	Correction: Saastamoinen model (Li et al., 2010a) Residual: Estimate as piece-wise mode
	Receiver clock error	Solved for at each epoch as white noise

tropospheric delay and phase ambiguity. The tropospheric delay is corrected using the tropospheric model and the rest of the wet part of the tropospheric delay is estimated by setting up a Piece-Wise Constant (PWC) at an interval of 1 h in data processing. In contrast to conventional PPP computation, the parameter of phase ambiguity is not used and only the ionosphere-free code combination is used in the code observable-based PPP. In data processing, the precise satellite clock and orbit products from IGS are used and corrections for Earth rotation, Earth tides and relativistic effects are implemented. The settings for the code observable-based PPP processing are shown in Table 1.

2.3. *Establishment of the stochastic model for the conventional PPP using the evaluated result.* It is important to use a reasonable stochastic model for GNSS processing and a reasonable selection for the ratio of the used phase and code observables is important to improve the PPP performance. The elevation-dependent function is generally written as:

$$w_j = \begin{Bmatrix} 1/\sigma^2 & 30^0 \le \theta_j \le 90^0 \\ 2\sin\left(\theta_j\right)/\sigma^2 & 10^0 \le \theta_j < 30^0 \end{Bmatrix} \tag{8}$$

where σ are the standard deviations in zenith of L1/L2 and P1/P2, respectively. The 1:100 for the ratio of the standard deviations for L1/L2 and P1/P2 is generally used (Hauschild and Montenbruck, 2009; Zhang et al., 2011). Considering the accuracy differences of the code observables selected by different GNSS receivers, the method for determining the ratio of the phase and code observables used is presented based on the evaluated results of the code observable. Assuming the ratio of the standard deviations for L1/L2 and P1/P2 is r, the standard deviation for the difference between the ionosphere-free carrier and code combinations can be written as:

$$\sigma_{dif} = \sqrt{\sigma_{ifp}^2 + r^2\sigma_{ifp}^2} = \sigma_{ifp}\sqrt{1+r^2} \tag{9}$$

Equation (9) can be also rewritten as:

$$r = \sqrt{\frac{\sigma_{dif}^2 - \sigma_{ifp}^2}{\sigma_{ifp}^2}} \tag{10}$$

According to Equation (6), the standard deviation of the differenced ionosphere-free carrier and code combinations can be computed. Thus, the ratio of the used phase and code

https://doi.org/10.1017/S0373463319000274 Published online by Cambridge University Press

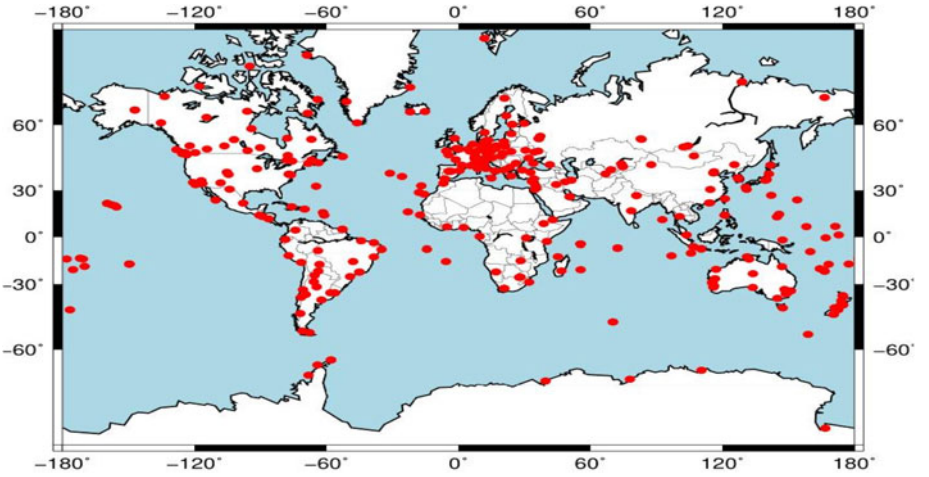


Figure 1. Distribution of the 342 IGS stations tracking GPS signals.

observables is computed, once the standard deviation of L1/L2 is known. This method fully takes into account the standard deviation difference of the different observations.

3. DATA PROCESSING. To analyse the performance of code observable-based PPP and the quality of the code observable collected by different GNSS receivers from ten manufacturers, a 24 hours dual-frequency GPS data set from 342 IGS stations collected from 27–28 October 2017 was processed. Data were sampled at 30 s and the cut-off elevation was set at 10°. Figure 1 shows the distribution of the 342 IGS stations used. The observable files of some stations collected by Ashtech receivers, parts of JPS, TPS and JAVAD receivers were created with the code smoothing option in TEQC turned off. In the code observable-based PPP and the conventional PPP processing, the final IGS orbit and clock products were used.

3.1. *Performance of the code observable.* Using Equation (6), the RMSs of the residuals of the differenced ionosphere-free carrier and code combinations for each tracked satellite were computed and the mean RMS for a receiver was obtained. The Mean RMSs for the code observable collected by different GNSS receivers are shown in Figure 2. The RMSs of the different GNSS receivers for the same brand were averaged and used to analyse the quality of the code observable for the corresponding brand of GNSS receiver. The mean RMSs for 10 brands of GNSS receivers are shown in Table 2. From Figure 2 and Table 2, it is observed that the qualities of the code observable of the Leica GNSS receivers are generally better than that of other receivers and the RMS of Leica GRX1200PRO reaches 0.71 m, although the C/A code observables are tracked. The Trimble receivers track the C/A code observables, which are similar to the Leica, but their RMS values are larger. The results of the three brands, JPS, TPS and JAVAD, in Table 2 show that the accuracy of code observables, which are created with the code smoothing option in Translation, Editing and Quality Checking (TEQC) turned off, are better than when turned on. From Figure 2, it can be seen that the results for the receivers JAVAD TRE_3 DELTA, JAVAD TRE_3N DELTA, JAVAD TRE_G3TH DELTA and TPS NET-G3A have the same performance. These results indicate that the quality of the code observable for the Ashtech brand is the

https://doi.org/10.1017/S0373463319000274 Published online by Cambridge University Press

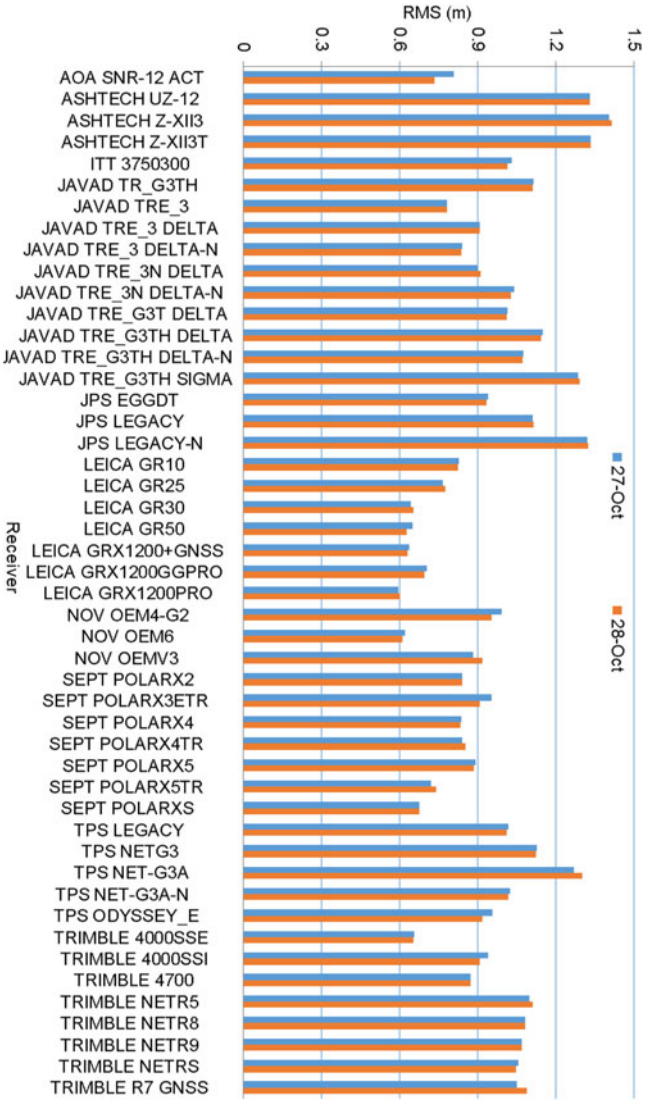


Figure 2. RMSs of different GNSS receivers. JAVAD TRE_3 DELTA-N, JAVAD TRE_3N DELTA-N, JAVAD TRE_G3TH DELTA-N, JPS LEGACY-N and TPS NET-G3A-N denote that the RMSs are computed using the observable files collected by the corresponding receiver and created with the code smoothing option in TEQC turned off.

worst in the ten brands and their RMS are greater than 1·2 m. However, it should be noted that the Ashtech files were created with the code smoothing option in TEQC turned off and the models Ashtech Z-XII3 and Ashtech UZ-12 are relatively old. Therefore, the Ashtech results may be due to ageing equipment and the application of relatively less modern technology. The RMSs of the 17 stations which used the LEICA GRX1200GGPRO and the different antennae are illustrated in Figure 3 and the corresponding antennae are shown in Table 3. Figure 3 and Table 3 indicate that there are differences between the qualities for the

https://doi.org/10.1017/S0373463319000274 Published online by Cambridge University Press

Table 2. RMSs for ten brands of GNSS receivers. JPS-N, TPS-N and JAVAD-N denote that the RMSs were computed using the observable files collected by the JPS, TPS and JAVAD receivers and created with the code smoothing option in TEQC turned off.

		RMS (m)				RMS (m)	
Brand	Tracked code	27 Oct	28 Oct	Brand	Tracked code	27 Oct	28 Oct
LEICA	C1 and P2	0·71	0·71	TPS-N	P1 and P2	1·02	1·01
AOA	P1 and P2	0·81	0·73	TPS	P1 and P2	1·16	1·17
NOV	C1 and P2	0·84	0·85	ITT	P1 and P2	1·03	1·01
SEPT	P1 and P2	0·85	0·85	JAVAD-N	P1 and P2	1·03	1·03
JPS-N	P1 and P2	1·00	1·00	JAVAD	P1 and P2	1·11	1·11
JPS	P1 and P2	1·11	1·11	TRIMBLE	C1 and P2	1·06	1·06
				ASHTECH	P1 and P2	1·34	1·34

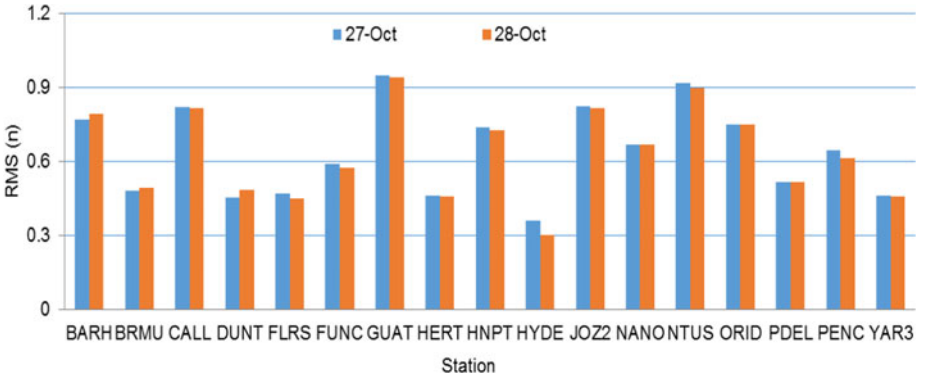


Figure 3. RMSs 17 stations which use LEICA GRX1200GGPRO and different antennae.

Table 3. Station and the antennae used.

Station	Antenna used
FLRS, FUNC, HERT, HYDE, JOZ2, NTUS, PDEL	LEIAT504GG NONE
CALL, NANO, ORID, PENC	LEIAT504GG LEIS
BARH, HNPT	LEIAX1202GG NONE
BRMU	JAVRINGANT_DM NONE
DUNT	LEIAT504 EIS
GUAT	LEIAR25·R3 LEIT
YAR3	LEIAR25 NONE

code observables collected from the different stations and antennae. This can be explained in that the space environments of different stations, which affect the code observables, are different and this includes the multipath effect.

3.2. *Performance of GPS code-based PPP.* Code observable-based PPP is implemented according to the settings shown in Table 1. In data processing, the station position, receiver clock and tropospheric delay are estimated in static and kinematic modes. The convergence time is defined as the elapsed time when the estimated coordinate errors in the North, East and Up directions are smaller than 10 cm when compared with the IGS results. The static results of the code observable-based PPP show that the 34 stations for

https://doi.org/10.1017/S0373463319000274 Published online by Cambridge University Press

27 October 2017 and 37 stations for 28 October 2017 can converge to the centimetre level over 24 h and the percentage is about 14%. The convergence times of these stations are shown in Table 4. The static positioning results of the CPVG, LCK4 and JPLM for 27 October and 28 October are illustrated in Figure 4. Table 4 indicates that the static positioning results of code observable-based PPP can converge to the centimetre level for all the brands of GNSS receivers, except the AOA. The JPLM station for 28 October has the best performance and its convergence time is about 2·5 h. The 47% centimetre level results are for the brands of Leica and Trimble, although these receivers tracked C/A code observables. The TRIMBLE NETR9 receiver had the highest number of the centimetre level results and the percentage was about 16%. The static results of the code observable-based PPP show that the Up direction has difficulty in converging to the centimetre level, compared with the North and East directions. The results for 27 and 28 October show that the performance of the code observable-based PPP is unstable, and it is irrelevant to the computed RMS values of the code observable. This can be verified from the results shown in Figure 4 and Table 4. The centimetre level results can be explained in that the errors in the ionosphere-free code combination have the statistical characteristics of random errors and can be reduced by averaging multiple observations. The mean value of the residual of the differenced ionosphere-free carrier and code combinations for each station at epoch m is computed as:

$$\widetilde{(\Delta)_m} = \sum_{k=1}^{n(m)} \left(\sum_{j=1}^{ep(k)} (\sigma_{1,2})_j \right)_k \Bigg/ \sum_{k=1}^{n(m)} ep(k) \tag{11}$$

where $ep(k)$ is the epoch number of the tracked satellite at epoch m and $n(m)$ is the satellite number of the tracked satellite at epoch m. The mean values at each epoch of the JPLM and LCK4 stations for 27 and 28 October are illustrated in Figure 5. Figure 5 shows that the residual of P1/P2 can converge to a stable value. In theory, this stable value is the effect of the code observation on code observable-based PPP and this can be verified by the results shown in Table 4 and Figures 4 and 5. The positioning results of JPLM for 28 October began to converge at epoch 300 and the corresponding mean value of the residuals of the differenced L1/L2 and P1/P2 reached zero. The mean value of the 24 h residuals of the differenced L1/L2 and P1/P2 for LCK4 of 28 October reach a stable value, which was about 0·3 m, while its 24 h positioning result in the Up direction does not converge to the centimetre level and is about 0·11 m. The results, which do not converge to the centimetre level, show there are biases in one or two and three directions, for example, the Up direction of the station LCK4 for 28 October in Figure 4 has an obvious and stable bias. The centimetre level results for 336 stations for 27 October and 339 stations for 28 October can be obtained, when the stable bias is removed. This bias, which is noticed in the same station and on a different date, can only be interpreted as the effect of the space environment. As to the studies on the stable bias, it is beyond the scope of this study.

The data from 27 and 28 October is also processed in kinematic mode and the station positions are estimated at each epoch using a least square filter. The results of the 342 stations are shown in Figure 6. From Figure 6, it is observed that the results for the North and East directions are better than that of the Up direction. The mean RMSs of the 342 stations for the North and East directions reaches the decimetre level and are 0·84 and 0·68 m, respectively, while that of the Up direction is 1·73 m. The Three-Dimensional (3D) RMS for each station was computed based on the RMS of the three directions to study

https://doi.org/10.1017/S0373463319000274 Published online by Cambridge University Press

Table 4. The convergence times of the static positioning.

Station	Convergence times (h)		Evaluation of the code observable (RMS, m)		Receiver	Antenna
	27 Oct	28 Oct	27 Oct	28 Oct		
ANKR	7·8	/	0·49	0·54	LEICA GR30	LEIAR10 NONE
BADG	20·0	17·8	1·14	1·15	JAVAD TRE_G3TH DELTA	JAVRINGANT_DM JVDM
BILB	21·7	21·6	1·73	1·75	ASHTECH Z-XII3	ASH701945E_M SCIS
BRMU	/	23·7	0·48	0·49	LEICA GRX1200GGPRO	JAVRINGANT_DM NONE
BSHM	7·2	22·3	0·79	0·79	JAVAD TRE_3 DELTA	TRM59800·00 SCIS
BZRG	14·0	/	0·83	0·83	LEICA GRX1200+GNSS	LEIAR25·R4 LEIT
CEDU	20·7	21·2	0·81	0·79	SEPT POLARX5	AOAD/M_T NONE
CHTI	/	20·2	0·98	0·98	TRIMBLE NETR9	TRM55971·00 NONE
CPVG	15·5	/	0·82	0·83	TRIMBLE NETR9	TRM59800·00 NONE
CRAO	15·1	22·6	1·40	1·40	ASHTECH UZ-12	ASH701945C_M SCIS
DRAG	22·0	/	0·92	0·91	JAVAD TRE_3 DELTA	ASH700936D_M SNOW
DUND	21·9	21·5	1·05	1·05	TRIMBLE NETR9	TRM57971·00 NONE
IENG	17·7	12·1	1·22	1·22	ASHTECH Z-XII3T	ASH701945C_M NONE
IPAZ	18·0	/	1·04	1·05	LEICA GR10	LEIAR10 NONE
ISBA	16·9	/	0·96	0·95	TRIMBLE NETR5	TRM57971·00 NONE
JOZ2	18·0	8·0	0·82	0·82	LEICA GRX1200GGPRO	LEIAT504GG NONE
JPLM	17·2	2·5	0·68	0·69	JPS EGGDT-N	AOAD/M_T NONE
KARR	14·4	12·4	1·12	1·12	TRIMBLE NETR9	TRM59800·00 NONE
KIRU	16·5	12·5	0·93	0·91	SEPT POLARX4	SEPCHOKE_MC SPKE
LAMA	23·9	18·5	0·60	0·54	LEICA GRX1200+GNSS	LEIAT504GG LEIS
LCK3	8·0	20·4	0·52	0·52	LEICA GRX1200+GNSS	LEIAR25·R3 LEIT
LCK4	15·6	/	0·53	0·53	LEICA GRX1200+GNSS	LEIAR25·R3 LEIT
MAT1	13·9	/	0·86	0·87	LEICA GR30	LEIAR20 NONE
MAUI	17·1	17·9	1·01	1·01	TRIMBLE NETRS	ASH700936D_M SNOW
M0SE	/	13·8	0·99	0·97	LEICA GR25	LEIAR25·R4 LEIT
MERS	/	11·8	0·28	0·33	LEICA GR5	LEIAR10 NONE
METS	/	9·2	1·08	1·10	JAVAD TRE_G3TH DELTA	ASH700936C_M ONE
MDO1	/	17·7	0·96	0·97	JAVAD TRE_G3TH DELTA-N	TPSCR·G3 SCIS
MOBN	19·9	/	1·44	1·47	ASHTECH UZ-12	ASH701945C_M SCIS
MQZG	18·1	17·5	1·23	1·23	TRIMBLE NETR9	TRM57971·00 NONE
MTV1	/	8·9	1·11	1·08	ITT 3750300	TPSCR·G5 TPSH
MTV2	/	9·2	1·12	1·09	ITT 3750300	TPSCR·G5 TPSH
NRMD	/	23·3	1·03	1·03	TRIMBLE NETR9	TRM57971·00 TZGD
POLV	19·5	18·7	0·50	0·49	LEICA GR10	LEIAR10 NONE
RABT	17·0	21·6	1·26	1·26	ASHTECH UZ-12	TRM29659·00 SCIS
RAMO	5·5	10·5	1·11	1·13	JAVAD TRE_G3TH DELTA	ASH701945B_M SNOW
SASS	/	14·6	1·09	1·04	JPS LEGACY	TPSCR3_GGD CONE
SNI1	17·3	17·1	0·62	0·60	TPS NET-G3A-N	TPSCR·G3 SCIS
STHL	/	20·8	0·82	0·82	JAVAD TRE_3 DELTA-N	TPSCR·G3 SCIS
SULP	/	6·0	1·32	1·33	TPS NET-G3A	TPSCR·G5 TPSH
SUTV	16·2	15·8	0·66	0·67	JPS EGGDT-N	ASH701945G_M NONE
TWTF	/	8·4	0·65	0·68	SEPT POLARX4	ASH701945C_M SCIS
URUM	/	18·8	0·78	0·78	JAVAD TRE_3	TPSCR3_GGD NONE
VNDP	21·9	15·7	1·11	1·10	TRIMBLE NETR9	TRM59800·00 SCIS
TAMP	23·9	/	1·11	1·10	LEICA GR10	LEIAR10 NONE
UNBN	23·8	/	0·62	0·61	NOV OEM6	TRM57971·00 NONE
WGTN	22·2	/	1·07	1·07	TRIMBLE NETR9	TRM57971·00 NONE
YAR2	11·1	11·3	0·61	0·60	SEPT POLARX4TR	AOAD/M_T NONE
ZECK	/	21·9	1·05	1·05	JAVAD TRE_G3TH DELTA	JAVRINGANT_DM JVDM

https://doi.org/10.1017/S0373463319000274 Published online by Cambridge University Press

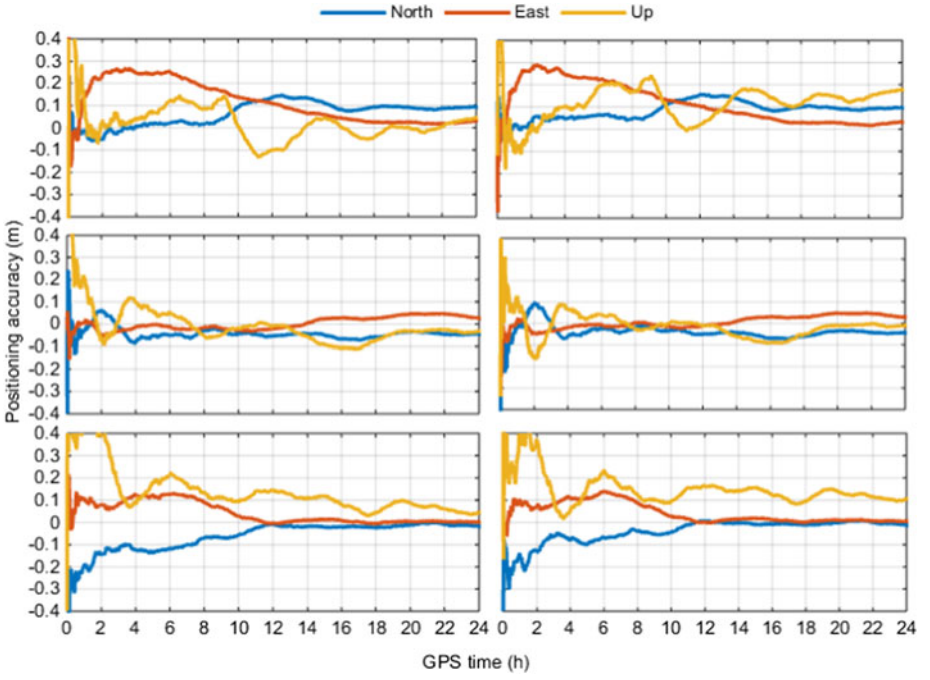


Figure 4. Accuracy of the code observable-based PPP for CPVG (top), JPLM (middle) and LCK4 (bottom) of 27 October (left) and 28 October 2017 (right).

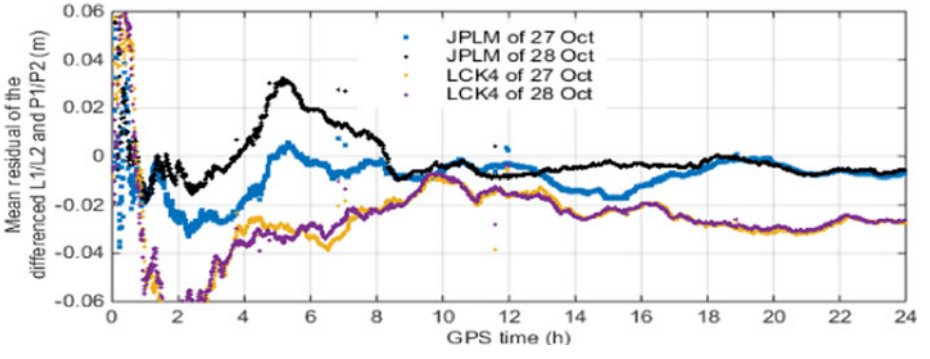


Figure 5. Mean values of the residual of the differenced L1/L2 and P1/P2 of the LCK4 and JPLM stations for 27 October and 28 October 2017.

the relationships of the accuracy for kinematic positioning and the evaluated results of the code observable. The 3D RMSs and the differenced L1/L2 and P1/P2 for each station are illustrated in Figure 7. Figure 7 shows that two types of RMS have similar trends. This demonstrates that the evaluated results of the code observable with the differenced L1/L2 and P1/P2 can reflect the performances of code observable-based kinematic PPP positioning.

3.3. *Performance of the presented stochastic model in conventional PPP.* The application of the code observable is meaningful for rapid and precise positioning, although it

https://doi.org/10.1017/S0373463319000274 Published online by Cambridge University Press

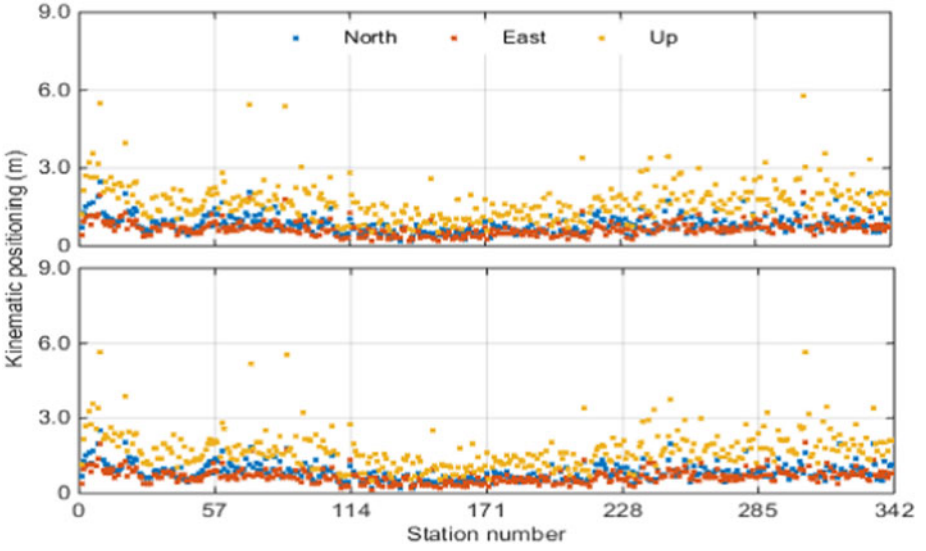


Figure 6. RMS of the kinematic positioning of the 342 stations 27 October (top) and 28 October 2017 (bottom).

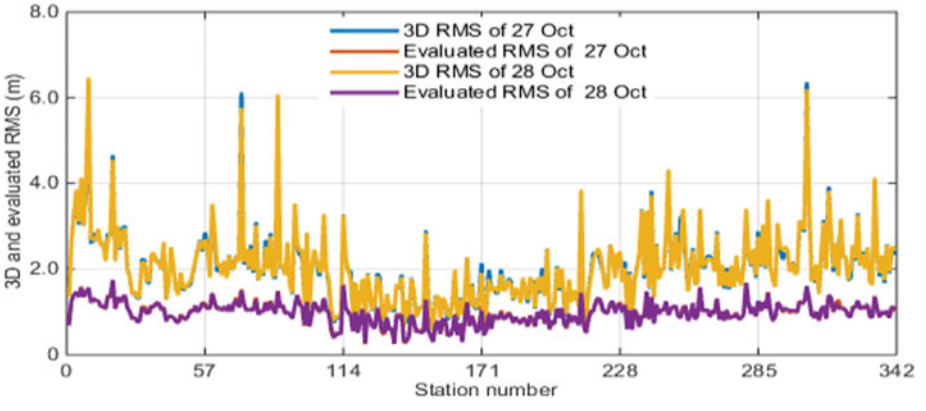


Figure 7. RMSs of 3D and evaluated results with differenced L1/L2 and P1/P2.

is considered that its accuracy is worse than that of the phase observable. The impact of the code observable in phase and code observables-based positioning dominates using the stochastic model. In current processing, the stochastic model is structured using the standard deviations of the phase and code observables. In fact, the standard deviations of the phase and code observables are used to determine the ratio of the contributions for the two types of observables in conventional PPP processing. The 1:100 ratio of the standard deviations for the phase and code observables in the stochastic model is generally used. This does not consider the accuracy difference and improvements of the GNSS receivers. The ratio of the standard deviations for L1/L2 and P1/P2 is computed according the method presented in Section 2.3 and used in conventional PPP processing. The shortened convergence time of the conventional PPP is computed using the difference between the convergence

https://doi.org/10.1017/S0373463319000274 Published online by Cambridge University Press

Table 5. The shortened convergence times for the static conventional PPP. The shortened convergence time is computed using the difference between the convergence times of the ratios of 1:100 and computed according to the proposed method.

	Shortened convergence times (min)		Evaluation of the code observable (RMS, m)			
Station	27 Oct	28 Oct	27 Oct	28 Oct	Receiver	Antenna
ABMF	2·5	/	0·95	0·94	LEICA GR25	TRM57971·00 NONE
AJAC	1·0	/	0·55	0·54	LEICA GR25	TRM57971·00 NONE
ALBH	/	1·0	1·04	1·06	TPS NET-G3A	TRM59800·00 SCIS
AMC2	1·5	331·5	1·32	1·35	ASHTECH Z-XII3T	AOAD/M_T NONE
ANKR	1·5	0·5	0·49	0·54	LEICA GR30	LEIAR10 NONE
ANTC	0·5	618·5	1·12	1·16	TRIMBLE NETR9	ASH700936D_M SNOW
AUCK	3·5	12·5	1·18	1·21	TRIMBLE NETR9	TRM57971·00 NONE
BJNM	6·5	/	1·03	0·99	SEPT POLARX3ETR	NOV702GG NONE
BOGI	2·5	/	1·02	1·01	JAVAD TRE_G3T DELTA	ASH701945C_M SNOW
BOR1	/	1·0	0·92	0·93	TRIMBLE NETR9	TRM59800·00 NONE
BRFT	/	1·0	0·59	0·60	LEICA GRX1200PRO	LEIAT504 NONE
BRMU	5·5	/	0·48	0·49	LEICA GRX1200GGPRO	JAVRINGANT_DM NONE
BRST	0·5	0·5	1·02	1·03	TRIMBLE NETR9	TRM57971·00 NONE
BRUX	/	0·5	0·66	0·66	SEPT POLARX4TR	JAVRINGANT_DM NONE
BSHM	/	0·5	0·79	0·79	JAVAD TRE_3 DELTA	TRM59800·00 SCIS
CAS1	/	3·5	1·04	1·05	TRIMBLE NETR9	LEIAR25·R3 LEIT
CATA	/	0·5	1·05	1·05	TRIMBLE NETR9	TRM55971·00 TZGD
CEBR	/	1·5	0·86	0·87	SEPT POLARX4	SEPCHOKE_MC NONE
CEDU	/	3·0	0·81	0·79	SEPT POLARX5	AOAD/M_T NONE
CHAN	31·0	4·5	1·27	1·28	ASHTECH UZ-12	ASH701945E_M NONE
COCO	/	14·0	0·51	0·51	SEPT POLARXS	AOAD/M_T NONE
CORD	2·0	/	1·03	1·01	JAVAD TRE_G3TH DELTA	TPSCR·G3 NONE
COYQ	/	1007·5	1·32	1·31	TRIMBLE NETR9	ASH700936D_M SNOW
CRAO	3·0	/	1·40	1·40	ASHTECH UZ-12	ASH701945C_M SCIS
DARW	/	4·0	1·09	1·08	SEPT POLARX5	JAVRINGANT_DM NONE
DUND	0·5	/	1·05	1·05	TRIMBLE NETR9	TRM57971·00 NONE
DYNG	0·5	1·0	0·83	0·84	TRIMBLE NETR9	TRM59800·00 NONE

times of the ratios 1:100 and computed according to the proposed method. In the conventional PPP processing, the standard deviations for the phase observable are set to a value of 0·01 m (Zhang et al., 2011) and the ratio of the standard deviations for L1/L2 and P1/P2 is computed based on this value. The results show that the convergence times for 80 stations for 27 October and 86 stations for 28 October 2017 can be accelerated and the percentage of station numbers is about 24%. The shortened convergence times for the static conventional PPP of some stations are shown in Table 5. The shortened convergence times verify that the presented method for improving the stochastic model of the conventional PPP is effective. They also indicate that the unified setting for the ratios of the standard deviations for L1/L2 and P1/P2 is not beneficial for rapid PPP processing and cannot achieve a full contribution of the code observable to the PPP result. These results indicate that a reasonable ratio should be used to structure the stochastic model for PPP processing. From Table 5, it is seen that the shortened convergence times for some stations, for example the AMC2, ANTC and COYQ stations, are significant and the shortened convergence times

https://doi.org/10.1017/S0373463319000274 Published online by Cambridge University Press

reach 331·5, 618·5 and 1007·5 min, respectively. When the presented stochastic model is used, the accuracy of this nearest direction is improved and is immediately better than 10 cm. The shortened convergence times of the two days show that the performances of the presented stochastic model are unstable and these unstable results can only be explained by the effect of the provided products.

4. CONCLUSION AND DISCUSSION. The accuracies of the GPS observables for the GNSS receiver, especially the code observable, improve with the development of the GNSS receiver technology. In PPP processing, the ionosphere-free carrier and code combinations are generally used to estimate the serviced products and the parameters of the PPP user side. Thus, the differenced ionosphere-free carrier and code combinations are used to evaluate the quality of the code observable. The evaluated results are used to develop a reasonable stochastic model. Considering improvement of the accuracy for the code observable, code observable-based PPP was implemented, and its performance was analysed. Two days of IGS data from 27–28 October 2017 was processed in the presented method. The two days' results show that the qualities of the code observable of Leica GNSS receivers were better than that of other receivers and the RMS of the Leica GRX1200PRO, which includes the multipath effect, reached 0·71 m, although it tracks the C/A code observables. The Trimble receivers track the C/A code observables, similar to the Leica receivers, but their RMS values are larger than those of the Leica receivers. However, the results of the code observable-based PPP show that the residuals of the ionosphere-free code combination for the Trimble receivers have a random error statistical characteristic and can be reduced by averaging multiple observations so that the corresponding static positioning has good performance.

The static results of code observable-based PPP for 34 stations for 27 October and 37 stations for 28 October can converge to the centimetre level in 24 h and the percentage for Trimble receivers is about 24%. On 28 October, the JPLM station shows the best performance of code observable-based PPP and its convergence time is about 2·5 h. From the results of the code observable-based PPP, it is seen that the Up direction has difficulty converging to the centimetre level, compared with the other directions of North and East. It is noticed that the performance of the code observable-based static PPP can be correlated with the accumulation characteristic of the errors of the code observable and the kinematic result can be correlated with the evaluated values. The shortened convergence times of conventional PPP show that the presented method for developing the stochastic model of PPP is meaningful and effective. The application of the evaluated results of the ionosphere-free code combination in the stochastic model of the conventional PPP indicates that a different stochastic model should be structured for the GNSS observations selected from different GNSS receivers and stations to obtain optimal PPP results.

ACKNOWLEDGEMENTS

This research is supported by the National Natural Science Foundation of China (NSFC) (No: 41674029), the Fundamental Research Funds for the Central Universities and the Key R&D Program (No: 2016YFB0501701).

https://doi.org/10.1017/S0373463319000274 Published online by Cambridge University Press

REFERENCES

Banville, S., Collins, P., Lahaye, F. (2013). GLONASS ambiguity resolution of mixed receiver types without external calibration. *GPS Solutions*, **17**(3), 275–282.

Bock, H., Dach, R., Jäggi, A. and Beutler, G. (2009). High-rate GPS clock corrections from CODE: Support of 1 Hz applications. Journal of Geodesy, **83**(11), 1083–1094.

Collins, P. (2008). Isolating and estimating undifferenced GPS integer ambiguities. *Proceedings of ION national technical meeting, San Diego, US*, 720–732.

Dow, J., Neilan, R. and Rizos, C. (2009). The International GNSS Service in a changing landscape of Global Navigation Satellite Systems. *Journal of Geodesy*, **83**(3–4), 191–198.

Estey, L.H. and Meertens, C.M. (1999). TEQC: the multi-purpose toolkit for GPS/GLONASS data. *GPS Solutions*, **3**(1), 42–49.

Fang, R., Shi, C., Song, W., Wang, G. and Liu, J. (2014). Determination of earthquake magnitude using GPS displacement waveforms from real-time precise point positioning. *Geophysical Journal International*, **196**(1), 461–472.

Ge, M., Gendt, G., Rothacher, M., Shi, C. and Liu, J. (2008). Resolution of GPS carrier-phase ambiguities in precise point positioning (PPP) with daily observations. *Journal of Geodesy*, **82**(7), 389–399.

Geng, J., Meng, X., Dodson, A.H. and Teferle, F.N. (2010). Integer ambiguity resolution in precise point positioning: method comparison. *Journal of Geodesy*, **84**(9), 569–581.

Geng, T., Xie, X., Fang, R., Su, X., Zhao, Q., Liu, G., Li, H., Shi, C. and Liu, J. (2016). Real-time capture of seismic waves using high-rate multi-GNSS observations: Application to the 2015 M_w7·8 Nepal earthquake. *Geophysical Research Letters*, **43**(1), 161–167.

Gao, Y. and Shen, X. (2002). A new method for carrier phase based Precise Point Positioning. *Navigation*, **49**(2), 109–116.

Hauschild, A. and Montenbruck, O. (2009). Kalman-filter-based GPS clock estimation for near real-time Positioning. *GPS Solutions*, **13**(3), 173–182.

Hilla, S. and Cline, M. (2004). Evaluating pseudorange multipath effects at stations in the National CORS Network. *GPS Solutions*, **7**(4), 253–267.

Kouba, J. and Héroux, P. (2001). Precise Point Positioning Using IGS Orbit and Clock Products. *GPS Solutions*, **5**(2), 12–28.

Kouba, J. (2005). A possible detection of the 26 December 2004 Great Sumatra Andaman Islands earthquake with solution products of the international GNSS service. *Studia Geophysica et Geodaetica*, **49**(4), 463–483.

Leick, A., Rapoport, L. and Tatarnikov, D. (2015) GPS satellite surveying, 4th edn. Wiley, New York.

Lannes A and Prieur J (2013) Calibration of the clock-phase biases of GNSS networks: the closure-ambiguity approach. *Journal of Geodesy*, **87**(8), 709–731.

Laurichesse, D. and Mercier, F. (2007). Integer ambiguity resolution on undifferenced GPS phase measurements and its application to PPP. *Proceedings of the 20th international technical meeting of the satellite division of the Institute of Navigation (ION GNSS 2007*), 839–848.

Leandro, R.F., Santos, M.C. and Langley, R.B. (2011). Analyzing GNSS data in precise point positioning software. *GPS Solutions*, **15**(1), 1–13.

Li, B., Shen, Y. and Xu, P. (2008). Assessment of stochastic models for GPS measurements with different types of receivers. *Chinese Science Bulletin*, **53**(20), 3219–3225.

Li, H., Chen, J., Wang, J., Hu, C. and Liu, Z. (2010a), Network based Real-time Precise Point Positioning. *Advances in Space Research*, **46**(9), 1218–1224.

Li, H., Wang, J., Chen, J., Hu, C. and Wang, H. (2010b). The realization and analysis of GNSS Network based Real-time Precise Point Positioning. *Chinese Journal of Geophysics-Chinese Edition*, **53**(6), 1302–1307.

Li, H., Chen, J., Wang, J. and Wu, B. (2012). Satellite- and epoch differenced precise point positioning based on regional augmentation network. *Sensors,* **12**(6), 7518–7528.

Li, H., Xu, T., Li, B., Huang, S. and Wang, J. (2016). A new differential code bias (C1–P1) estimation method and its performance evaluation. *GPS Solutions*, **20**(3), 321–329.

Loyer, S., Perosanz, F., Mercier, F., Capdeville, H. and Marty, J.C. (2012). Zero difference GPS ambiguity resolution at CNES-CLS IGS analysis center. Journal of Geodesy, **86**(11), 991–1003.

Seepersad, G. and Bisnath, S. (2015). Reduction of PPP convergence period through pseudorange multipath and noise mitigation. *GPS Solutions*, **19**(3), 369–379.

Shi, J., Yuan, X., Cai, Y. and Wang, G. (2017). GPS real-time precise point positioning for aerial triangulation. *GPS Solutions*, **21**(2), 405–414.

https://doi.org/10.1017/S0373463319000274 Published online by Cambridge University Press

Teunissen, P.J.G., Odijk, D. and Zhang, B. (2010). PPP-RTK: results of CORS network-based PPP with integer ambiguity resolution. *Journal of Aeronautics, Astronautics and Aviation*, **42**(4), 223–229.

Teunissen, P.J.G. and Khodabandeh, A. (2015). An analytical study of PPP-RTK corrections: precision, correlation and user-impact, Journal of Geodesy, **89**(11), 1109–1132.

Wang, J., Stewart, M. and Tsakiri, M. (1998). Stochastic Modeling for Static GPS Baseline Data Processing. *Journal of Surveying Engineering*, **124**(4), 171–181.

Zhang, X., Li, X. and Guo, F. (2011). Satellite clock estimation at 1 Hz for realtime kinematic PPP applications. *GPS Solutions*, **15**(4), 315–324.

Zhang, X., Li, P. and Guo, F. (2013). Ambiguity resolution in precise point positioning with hourly data for global single receiver. Advances in Space Research, **51**(1), 153–161.

Zumberge, J.F., Heflin, M.B., Jefferson, D.C., Watkins, M.M. and Webb, F.H. (1997) Precise point positioning for the efficient and robust analysis of GPS data from large networks. *Journal of Geophysical Research*, **102**(B3), 5005–5017.

https://doi.org/10.1017/S0373463319000274 Published online by Cambridge University Press